ISIJ International, Vol. 56 (2016), No. 5, pp. 828–834

Structural Characterization of $FeO–SiO_2–V_2O_3$ Slags Using Molecular Dynamics Simulations and FT-IR Spectroscopy

Zhen ZHANG, Bing XIE,* Wang ZHOU, Jiang DIAO and Hong-Yi LI

College of Materials Science and Engineering, Chongqing University, No. 174 Shazhengjie Street, Shapingba District, Chongqing, 400044 China.

(*Received on October 19, 2015; accepted on January 5, 2016; J-STAGE Advance published date: April 5, 2016*)

The structure of $FeO–SiO_2–V_2O_3$ slags with compositions of $(1-x)(1.5FeO{\cdot}SiO_2){\cdot}xV_2O_3$ (x=0–20% mole fraction) was investigated in the molten and quenched states by using molecular dynamics (MD) simulations and Fourier transform infrared (FT-IR) spectroscopy. An empirical potential for the multi-component system has been developed in this work for performing MD simulations. The local atomic structures and the micro-heterogeneity in the molten slag have been systematically investigated using MD simulations. The bond length of V–O varies from 1.92 to 1.96 Å and the averaged coordination number of V ($CN_{V–O}$) increases from 4.50 to 4.96 with the addition of V_2O_3. The simulation results revealed that the average Si–O–Si bond angle and the degree of polymerization both decrease with increasing amount of V_2O_3, implying that V_2O_3 may behave as a network-modifying basic oxide in the $FeO–SiO_2–V_2O_3$ system. This was further confirmed by the FT-IR spectrum analysis, which shows that the silicate network dissociates with the presence of V_2O_3.

KEY WORDS: $FeO–SiO_2–V_2O_3$; slag structure; molecular dynamics simulations; FT-IR.

1. Introduction

Vanadium-titanium (V–Ti) magnetite ore is one of the most extensively utilized resources for vanadium extraction.[1)] To extract valuable metal from the V–Ti magnetite, a typical blast furnace-LD converter process is adopted in China.[2)] In this process, V-containing hot metal will be oxidized in a LD converter to produce vanadium slag, which is an important intermediate product of vanadium extraction from V–Ti magnetite. Investigating the structure of molten slag is of great help for understanding and controlling the properties of slag such as viscous flow,[3,4)] which is also a significant thermophysical property for vanadium slag since it will influence the slag-metal separation as well as oxidation of vanadium from the hot metal into the slag.[2,5)]

Fe and V are both transition elements that can exist in variable oxidation states and structural environments under different internal or external conditions. Carmichael and Ghiorso[6)] reported that only V^{3+} is the stable species in most silicate melts under terrestrial oxygen fugacity (fO_2). Previous mineralogical phase studies of plant and synthetic vanadium slags show that spinel phase (FeV_2O_4) is the main host of V, while Fe exists in both silicate phases (M_2SiO_4 or $MSiO_3$, where M represents Fe^{2+}, Mn^{2+} and Mg^{2+}.) and spinel phase, meaning that the valences of V and Fe in the vanadium slag system are mostly +3 and +2 respectively.[5,7–11)] Recently, Fang[12)] modelled the thermodynamic behavior of Fe, V and Cr in molten slag. It was found that under the conditions of practical refining of V-containing hot metal, where the $\log(fO_2)$ varies from −11 to −10 at the slag-metal reaction interface, the oxide forms of V and Fe can be assigned as $VO_{1.5}$ and $FeO_{1.05}$. Based on these theoretical and experimental results, here in this study, we only consider the V^{3+} and Fe^{2+} exist in the vanadium slag and the possible valence transformations induced by compositional variation are not taken into consideration for clarity and simplification.

The structure of ferrosilicate-based melts and glasses has been extensively investigated through diffraction (scattering) and spectroscopic methods.[13–18)] Meanwhile, molecular dynamics (MD) simulation, as a approach complementary to experimental techniques, has also been applied to investigate the structure and properties of ferrosilicate systems.[14,19,20)] Both experimental and simulation work have suggested that SiO_4 tetrahedron is the fundamental building block for silicates, while the structural behavior of Fe^{2+} is still debated. Fe^{2+} adopts 4-, 5- or 6-fold coordination were found in silicate melts and glasses under different silicate composition, temperature, pressure and fO_2.[14–16,18,21–25)] Notwithstanding, in most cases FeO acts as a network modifier which offers O^{2-} and thus depolymerizes the silicate network.[4,15)]

Although there are numerous studies on the structural characterization and physicochemical properties of V-containing materials, rather limited information is available on the structural configurations of trivalent V in silicate melts and glasses. To the authors' knowledge, only Keppler[22)] reported that V^{3+} occupies octahedral coordination in

* Corresponding author: E-mail: bingxie@cqu.edu.cn
DOI: http://dx.doi.org/10.2355/isijinternational.ISIJINT-2015-600

glasses along the diopside-albite join by using optical spectroscopy. The structural information of silicate melts and glasses containing both Fe^{2+} and V^{3+} has not been reported yet.

In the present work, we focus on $FeO–SiO_2–V_2O_3$ (FSV) system that represents the major components of vanadium slag.[2] The aim of this study is to characterize the structural features of V_2O_3-contining molten slags and hopefully clarify the microscopic behavior of V_2O_3 in this system. For this purpose, we firstly developed an effective empirical pair potential for the FSV system. Then classical MD simulations and FT-IR experiments were performed to investigate the structural characteristics of FSV slags with varying V_2O_3 content up to 20% at a fixed FeO/SiO_2 molar ratio of 1.5. Analogous compositional selection and research approaches have been adopted in recent structural and viscosity studies of $CaO–SiO_2–TiO_2$ system.[27,28]

2. Simulation Details

The Born-Mayer-Huggins (BMH) potential, which has been successfully used to describe the interactions between ions of ferrosilicate melts and glasses,[14,19,20] was applied to simulate the FSV system. This ionic potential consists of the long-range Coulomb, the short-range repulsive and van der Waals (attractive dipole-dipole) interactions. The general expression for potential between two atoms *i*-*j* is:

$$V(r_{ij}) = \frac{q_i q_j e^2}{4\pi\varepsilon_0 r_{ij}} + A_{ij}\exp\left(-\frac{r_{ij}}{B_{ij}}\right) - \frac{C_{ij}}{r_{ij}^6} \quad \text{..... (1)}$$

where, i and j are atom species (Si, O, Fe, or V), q_i is the effective charges on atom i. r_{ij} is the distance between the pair ij, e is the electron charge, ε_0 is the vacuum permittivity, and A, B, and C are the potential parameters which can be empirically determined by fitting the crystal structures and other properties. The ionic charges follow the setup: +2 for Fe, +4 for Si, +3 for V and −2 for O. All van der Waals interaction are treated as zero, namely, C_{ij} is zero, to improve the numerical optimization efficiency during parameters fitting.

The reliability of MD simulations greatly depends on the accurate description of the interatomic interactions. In this work, the interaction potential parameters of SiO_2 were taken from the well-established one by Hirao and Kawamura,[29] and the potential parameters for other species interaction were developed by empirically fitting the structure and physical properties of relevant crystals of FSV system (**Table 1**). These potential parameters have been evaluated using the LAMMPS package.[30] The experimental structural parameters such as lattice parameters (a, b, c, α, β, γ) and molar volume (V) were well reproduced within negligible deviation as shown in **Table 2**, demonstrating the reliability of the pair potential parameters we adopted.

Random initial configurations and periodic boundary conditions were applied to the basic cells containing approximately 4 000 atoms. Canonical ensemble (NVT) was adopted for all simulations in this study. The long-range Coulombic interactions were calculated using the Ewald summation method with an accuracy of 10^{-5} and a cutoff of 10 Å. The equation of motion was integrated by the fifth-order Gear's predictors-corrector algorithm with a time step of 1.0 fs. The calculation was carried out at a constant pressure of 101 kPa and temperature was controlled with the velocity scaling method. The temperature was initially set to 4 000 K for 30 000 time steps to eliminate the effect of the initial distribution on the final structure. Then, the temperature was decreased to 1 823 K with a cooling rate of 0.1 K per step. The temperature was fixed at 1 823 K for 50 000 time steps to achieve equilibrium, and the structural data were accumulated for microscopic structural analysis during the last 10 000 time steps.

The compositions and other details of the model are

Table 1. Parameters of BMH potentials used in this study.

Atom pair	A_{ij} (eV)	B_{ij} (Å)
Fe–Fe	2 933.34	0.2900
Fe–V	2 186.50	0.2139
Fe–O	40 000.00	0.1937
V–V	7 391.98	0.2432
V–O	1 830.20	0.3061
O–O	1 497 526.22	0.1700
Si–O	62 814.39	0.1650
Si–Fe	5 754.57	0.0775
Si–V	4 547.21	0.2900
Si–O	2 163.08	0.1600

Table 2. Comparison between experimental and calculated structures of relevant crystals.

	αSiO_2 (P3221)		FeO (Fm-3m)		Fe_2SiO_4 (Pnma)		V_2O_3 (R3-ch)		FeV_2O_4 (FD-3m)	
	Exp.[31]	Calc.	Exp.[32]	Calc.	Exp.[33]	Calc.	Exp.[34]	Calc.	Exp.[35]	Calc.
a (Å)	4.913	4.855	4.326	4.313	10.460	10.407	4.952	4.992	8.543	8.548
b (Å)	4.913	4.855	4.326	4.313	6.082	6.138	4.952	4.992	8.543	8.548
c (Å)	5.405	5.277	4.326	4.313	4.815	4.867	14.002	13.605	8.543	8.548
α (°)	90	90	90	90	90	90	90	90	90	90
β (°)	90	90	90	90	90	90	90	90	90	90
γ (°)	119.23	119.99	90	90	90	90	120	120.66	90	90
V(10^{-6} m^3/mol)	112.96	121.44	81.30	80.25	306.32	310.93	297.36	298.80	623.49	624.59

Table 3. Slag composition, simulation cell sizes, and density.

Slag	Composition (mol-%)			Number of atoms					Cell size (Å)	Density (g/cm^3)
	FeO	SiO_2	V_2O_3	Fe	Si	O	V	Total		
FSV0	60.0	40.0	0.0	1 000	667	2 333	0	4 000	38.25	3.321
FSV04	57.6	38.4	4.0	920	613	2 338	128	3 999	38.02	3.399
FSV08	55.2	36.8	8.0	847	565	2 345	246	4 002	37.83	3.472
FSV12	52.8	35.2	12.0	779	519	2 349	354	4 001	37.63	3.543
FSV16	50.4	33.6	16.0	716	477	2 353	455	4 001	37.46	3.609
FSV20	48.0	32.0	20.0	657	438	2 354	548	3 997	37.28	3.673

Table 4. Slag samples compositions from XRF (mol-%).

Samples	FeO/SiO_2	FeO	SiO_2	V_2O_3
1#	1.55	60.8	39.2	–
2#	1.51	58.4	38.8	2.9
3#	1.47	54.3	37.0	8.7

shown in **Table 3**. It is necessary to note that there is no experimental density data available for the V_2O_3-containing slags. Therefore, in this study the empirical formula from literature[36] has been adopted to calculate the density of FSV slags, and the thermal expansion rate of V_2O_3 at simulation temperature is set as a typical value, 5%.

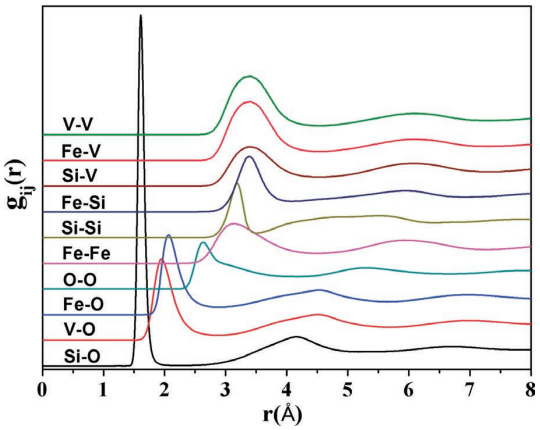

Fig. 1. Pair distribution functions of FSV12. (Online version in color.)

3. Experimental Procedures

Analytical-grade chemicals of SiO_2, V_2O_3 and FeO that was prepared through pyrolysis of $FeC_2O_4{\cdot}2H_2O$ (≥98.0%) at 600°C in a vertical vacuum electric furnace were used to synthesize slag samples. About 50 g of sample with different compositions were charged into a molybdenum crucible (diameter 40 mm, depth 65 mm) and melted in a $MoSi_2$ high temperature furnace at 1 550°C for more than 2 hours to obtain homogeneous molten slag. All FeO preparation and sample melting process were conducted under 1.0 L/min of purified Ar to minimize potential oxidization. Afterwards, the molten slag were rapidly taken out from the furnace and quenched by liquid nitrogen to get glassy sample.

The slag compositions of quenched slags determined by x-ray fluorescence (XRF) spectroscopy (S4 Explorer; Bruker AXS GmbH, Karlsruhe, Germany) are shown in **Table 4**. To examine the structure of FSV slags qualitatively, the quenched slag samples were finally analyzed using FTIR spectroscopy (Nicolet iS50, Thermo Scientific, USA) in the range of 4 000 to 400 cm^{-1}.

4. Results and Discussion

4.1. Local Structure of the Melts

Insight into the local structure in the molten slag can be achieved by analyzing the pair distribution functions (PDFs),

$$g_{ij}(r) = \frac{V}{N^2}\left\langle \sum_{i=1}^{N} \sum_{j=1,i\neq j}^{N} \delta(r - R_{ij}) \right\rangle \quad \text{..... (2)}$$

where, V is the volume of the system and N the number of atoms. $\langle\bullet\rangle$ denotes averaging. For atoms i and j, Eq. (2) gives the normalized averaged distribution of atom i around a central j atom within a determined cut-off distance. As an example, the calculated PDFs for the FSV12 slag have been plotted in **Fig. 1**.

The bond lengths determined from the first peak positions of the corresponding PDFs as well as those experimental values in similar molten and glassy silicate systems are detailed in **Table 5**. Waseda[13] studied the short-range ordering in ferrosilicate melts using high temperature X-ray diffraction and it was found that the bond lengths for Si–O and Fe–O pairs are around 1.62 and 2.05 Å, respectively. Our simulations satisfactorily agree with Waseda. The Si–Si bond length obtained from our MD simulations (around 3.19 Å) is successfully comparable to the experimental values (3.18–3.24 Å) of molten ferrosilicates[13] but somewhat longer than the values (3.08 Å) observed in glassy silicates,[37] implying a different inter-tetrahedral connectivity may be found for silicates in differently existing states.

To the best of our knowledge, the V–O bond length in molten or glassy slag system has not been reported so far. A direct comparison is therefore unfeasible. Our simulated results show that the V–O bond length increases with the addition of V_2O_3 from 1.92 to 1.96 Å, indicating a possible structural environmental change of V. This is supported by a slight increase of the O–O bond length from 2.62 to 2.64 Å with increasing the content of V_2O_3.

The local structure can be further investigated through analyzing the coordination numbers (CNs) and the bond-angle distributions (BADs). The CNs are obtained by counting the number of particular atoms in the atomic con-

Table 5. Bond lengths (Å) of the simulated slags and those from experiments.

Pairs	FSV0	FSV4	FSV8	FSV12	FSV16	FSV20	Exp.
Si–O	1.61	1.61	1.61	1.61	1.61	1.61	1.62–1.63,[13] 1.62[37]
Fe–O	2.05	2.06	2.06	2.07	2.07	2.07	2.04–2.08,[13] 1.99[14]
V–O	–	1.92	1.95	1.95	1.96	1.96	
O–O	2.62	2.62	2.63	2.64	2.64	2.64	2.63[37]
Si–Si	3.19	3.19	3.19	3.19	3.19	3.18	3.18–3.24,[13] 3.08[37]

Table 6. Selected averaged coordination numbers and averaged bond-angles (degree).

	FSV0	FSV4	FSV8	FSV12	FSV16	FSV20
CN_{Si-O}	4.01	4.02	4.01	4.02	4.02	4.00
CN_{Si-NBO}	2.34	2.65	2.77	2.88	3.03	2.98
CN_{Fe-O}	4.63	4.85	4.93	5.03	5.10	5.12
CN_{V-O}	–	4.50	4.74	4.91	4.94	4.96
CN_{Si-Fe}	5.79	5.66	5.48	5.33	5.03	4.86
CN_{Si-V}	–	0.65	1.35	1.81	2.58	3.10
CN_{Fe-Fe}	6.55	6.05	5.69	5.31	5.19	4.82
CN_{V-V}	–	0.86	1.84	3.09	3.77	4.58
θ_{O-Si-O}	109.29	109.28	109.28	109.28	109.26	109.26
$\theta_{Si-O-Si}$	154.99	152.30	153.25	151.88	150.48	151.08

figurations with a cutoff corresponding to the first valley position of the corresponding PDFs. In this study, the cutoff values for Si–O, Fe–O and V–O pairs are fixed at 2.00, 2.90 and 2.85 Å, respectively. While the cutoff values for other cation-cation pairs are moderately changed with respect to the variation of slag compositions.

For Si–O bonds, the CN of Si (CN_{Si-O}) stabilized at around four suggests its role of network former and the high field strength (see **Table 6**). Nevertheless, with respect to the contributions from bridge oxygen (BO, Oxygen atoms that are shared between two SiO_4-tetrahedron) and non-bridge oxygen (NBO, Oxygen atoms that are bonded to only one Si and another cation), the contribution from NBO tends to increase with the addition of V_2O_3. It is noteworthy that the number of oxygen in our simulation boxes remains almost the same for all the simulated compositions as shown in Table 3. The increasing contribution from NBO to CN_{Si-O} indicates that the amount of NBO tends to augment while that of BO decreases with V_2O_3 addition.

Further information about the Si–O coordination shell can be obtained by examining the BADs. The O–Si–O BAD shown in **Fig. 2**(a) displays a main peak around 109° and no distinct compositional dependence is observable. These peak values are close to the angle of a perfect tetrahedron, 109.47°, supporting the stable 4-fold coordination structure of Si. The Si–O–Si BAD in Fig. 2(b) reveals the connection between SiO_4 tetrahedrons. A wide distribution of the Si–O–Si angle from ~120° to 180° is consistent with the reported results.[38,39] According to previous studies,[43,48] the introduction of a modifier will cause the decrease of the Si–O–Si angle in the silicate network. The average angle of the Si–O–Si, listed in Table 5, slightly decreases from

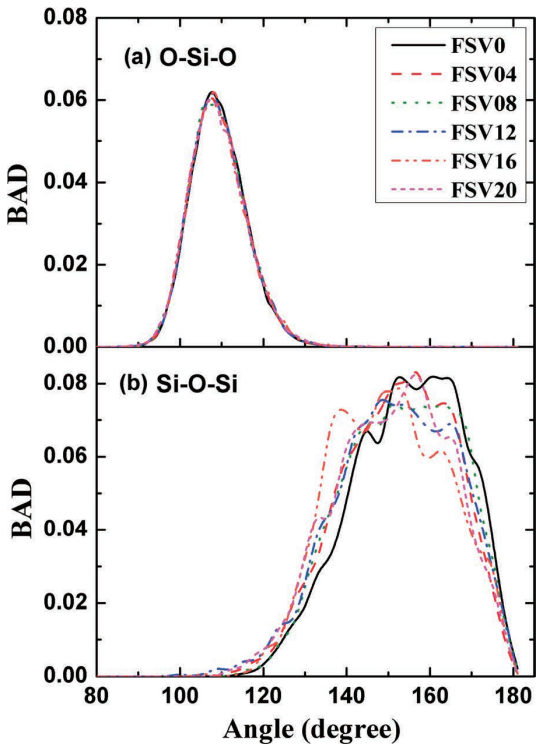

Fig. 2. Bond angle distributions of (a) O–Si–O and (b) Si–O–Si. (Online version in color.)

~155° to 151° with increasing the V_2O_3 content, this may be an indication that V_2O_3 act as a modifier in this tetrahedral network.

The averaged CN of Fe (CN_{Fe-O}) increases consistently with increasing the V_2O_3 concentration (Table 6), ranging from 4.63 to 5.12. The distribution of CN of Fe–O bonds (**Fig. 3**(a)) shows a rather broad distribution ranging from 3 to 7, most of which are 4, 5 and 6 corresponding to tetrahedral, pyramidal and octahedral structural units, respectively. With the addition of V_2O_3, the percentage of Fe in 4-fold coordination decreases from around 40% for FSV0 to 18% for FSV20, while that of the Fe in 6-fold coordination grows from around 13% to 28%. Generally, cations with 6-fold coordination (in octahedral array) are more likely to act as network breakers (or network modifiers) compared to 4- or 5-fold coordinated ones in silicate systems.[4] Therefore, the variation in the coordination of Fe^{2+} may imply that the network-modifying effect of Fe^{2+} on the Si–O network is enhanced by the addition of V_2O_3. The existing structural positions of Fe^{2+} in our simulations are in accordance with previous studies,[15,16,18,21–26] in spite of the investigated silicate systems may vary from one to the other.

For V–O bonds, analogous to Fe–O bonds, the percentage

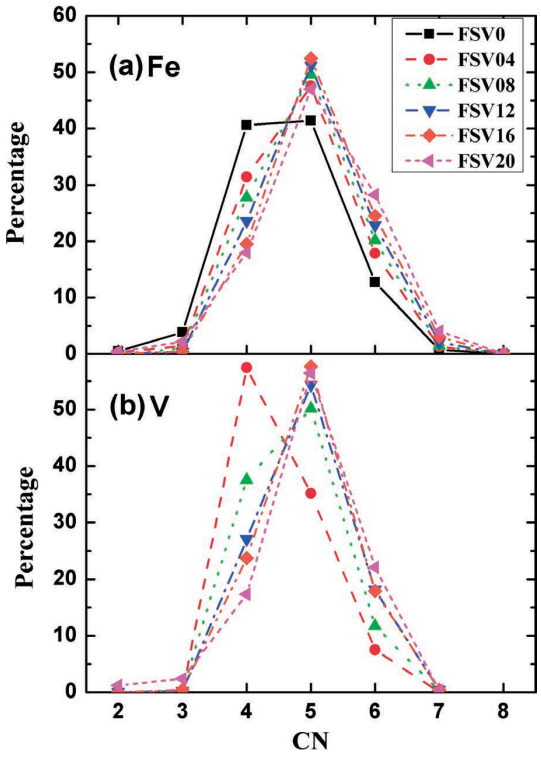

Fig. 3. Distribution of the coordination numbers of (a) Fe–O and (b) V–O bonds. (Online version in color.)

of the 6-fold coordinated V increases while the 4-fold coordinated V decreases with respect to the V_2O_3 addition (Fig. 3(b)). Overall the CN of V (CN_{V-O}) increases from 4.50 to 4.96 and the 5-coordinated V becomes predominant for the V–O coordination. Keppler[22] investigated the coordination chemistry of transition metal ions in silicate systems by crystal field spectral analysis. It was found that V^{3+} occupies octahedral site in the glasses. However, considering only a slight amount of V_2O_3 (0.1 mass pct) was doped in the glasses, Keppler's results are therefore incomparable with our simulated results. Nevertheless, the range of CN_{V-O} between 4.50 and 4.96 fits well into the results detected in other vanadium (tetravalent and pentavalent vanadium) containing glasses.[40,41]

4.2. Microheterogeneity in the Molten Slag Structure

In addition to the local structural analysis, determining the spatial distribution of ions can be an effective way of characterizing the heterogeneity in the slag structure. Note that here microheterogeneity means segregation or clustering of cations in the slag melts. By using particular characterization methods, we evaluate the distribution and segregation of ions, especially Fe and V, in FSV molten slags.

The CN of Fe or V around Si (CN_{Si-Fe} or CN_{Si-V}) is presented in Table 6. It can be seen that the CN_{Si-Fe} decreases linearly while CN_{Si-V} increases with increasing concentration of V_2O_3. The linear changes of CN_{Si-Fe} and CN_{Si-V} can be attributed to the variations of the number density of Fe and V ions in the simulation boxes. To investigate the preference for Fe and V ions around Si, we adopt the ratio R,[42]

$$R^{A}_{B/C} = \frac{CN_{A-B}}{CN_{A-C}} \times \frac{N_C}{N_B} \quad \text{..... (3)}$$

where, A stands for the network former, namely Si in this study; CN_{A-B} represents CN of ion B around a central ion A (see Table 6); N_B is the number of ion B in the simulation cell which can be learned from Table 3. When the ratio R is close to 1, B and C distribute statistically around A, which means that A has no preference for B or C. Yet, a ratio of R greater than 1 denotes the performance for B ions, whereas a ratio less than 1 suggests performance of A for coordination of C. As the calculated values of R shown in **Table 7**, it can be seen that Si as the central ion prefers Fe more within its first coordination shell in all slag compositions compared to V, and the preferential degree of cations around Si is insensitive to the changes of the V_2O_3 content. The network-forming Si prefers Fe to V is in tune with the trend of the CNs of cations (Table 6), where CN_{Si-Fe} is consistently larger than CN_{Si-V} along the investigated composition range, demonstrating a stronger ability of Fe attracting O from the Si–O network compared to V.

Table 7. Parameters for characterizing the microheterogeneity of the FSV slags.

		FSV0	FSV4	FSV8	FSV12	FSV16	FSV20
$R^{Si}_{Fe/V}$		–	1.21	1.18	1.34	1.24	1.31
R^{obs}_{hom}	SiFe	1.11	1.13	1.16	1.19	1.20	1.23
	SiV	–	1.00	1.03	0.95	1.00	0.96
	FeFe	1.13	1.15	1.18	1.19	1.23	1.28
	VV	–	–	3.09	2.01	1.67	1.55

Aside from the preference for different cations (Fe and V) around network former (Si), the distribution of cations, clustering or homogeneous, provides us important information about the medium-range structure and the trend of ion aggregation in slag melt. Here we characterize the clustering behavior of cations by using a specific ratio R^{obs}_{hom},[42,43]

$$R^{obs}_{hom} = \frac{CN_{obs}}{CN_{hom}} \quad \text{..... (4)}$$

$$A-B\ pairs: CN_{hom} = \frac{4\pi R_c^3}{3} \times \rho_0$$
$$A-A\ pairs: CN_{hom} = \frac{4\pi R_c^3}{3} \times \rho_0 - 1 \quad \text{..... (5)}$$

where, CN_{obs} corresponds to the values listed in Table 6; CN_{hom} is the theoretical CN calculated from a homogeneous distribution of ions. ρ_0 denotes the number density of coordinating ion and R_c equals the cutoff values used in CN_{obs} calculation. Consequently, the R^{obs}_{hom} value that is larger than 1 indicates that the tendency of ion segregation exists while a homogeneous distribution of ions can be deduced if the R^{obs}_{hom} ratio is close to 1.

For the distribution of Fe ions, Fe around Si (SiFe) and Fe around Fe (FeFe) show similar trend of segregation as reflected by the R^{obs}_{hom} values (Table 7), where the segregation exists and the tendency of segregation slightly increases with the addition of V_2O_3. The R^{obs}_{hom} ratios for V around Si (SiV) show no obvious changes with a value close to 1, demonstrating a homogeneous distribution of V ions around Si in the slags. By contrast, as the V_2O_3 content increases, the clustering tendency of V around V (VV) decreases con-

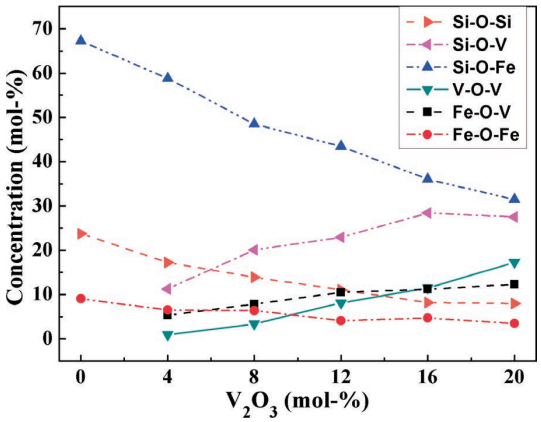

Fig. 4. Concentration of the different types of O versus the mole fraction of V_2O_3. (Online version in color.)

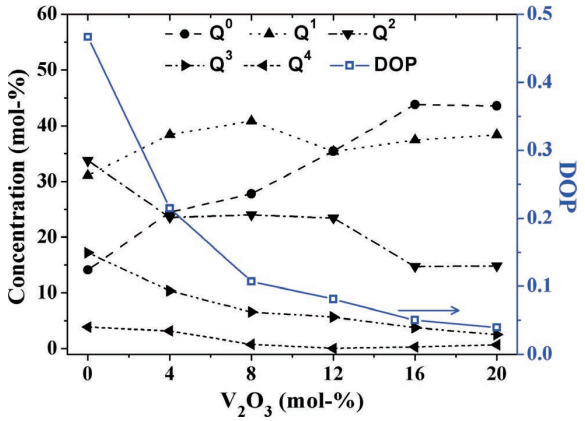

Fig. 5. Distribution of the Q^n of Si versus the mole fraction of V_2O_3. (Online version in color.)

siderably since the R_{hom}^{obs} ratios for VV decline continuously. This might be a structural origin of changes in the macro-properties of the FSV slags.

4.3. Effect of V_2O_3 on the Network Connectivity

Analyzing the different types of oxygen in the slags plays a prominent role on characterizing the structural properties. Here we classify oxygen atoms by the cations connected to one oxygen. As demonstrated in **Fig. 4**, the fraction of Si–O–Si that corresponds to BO drops from 24% to 8% monotonically, suggesting the depolymarization of the network. In contrast, the concentrations of Si–O–Fe and Si–O–V increase with the addition of V_2O_3. The interactions between different cation-oxygen bonding can be described by Eqs. (6) and (7).

$$(Si-O-Si)+(V-O-V)\leftrightarrow 2(Si-O-V) \quad \text{..... (6)}$$

$$(Si-O-Fe)+(V-O-V)\leftrightarrow (Si-O-V)+(Fe-O-V) \quad \text{..... (7)}$$

Furthermore, information on the network connectivity of the melts can be obtained by analyzing the Q^n species distribution, where n is the number of BO linked to one SiO_4 tetrahedron, $n=0,1,2,3,4$. The concentrations of each Q^n species were determined based on the configurational statistical results of 4-fold coordinated Si atoms with different number of BO. **Figure 5** shows that with the addition of V_2O_3, the Q^0 and Q^1 species become dominate in the distribution. This change is in contrast to the decrease of Q^3 and Q^4 species, implying the depolymerization of the network. Also, due to the relatively low content of SiO_2 in our studied system, only a small amount of Q^4 specie was found (less than 5%) for all slags.

Here we characterize the degree of polymerization (DOP) by using the definition that $DOP=(Q^3+Q^4)/(Q^1+Q^0)$. As shown in Fig. 5, the DOP decreases dramatically with increasing the concentration of V_2O_3 from 0 to 8% and then decreases gradually if further increase the V_2O_3 content, demonstrating a decline of the cross-linking degree of the SiO_4 tetrahedral network, in accordance with our previous statements.

To further validating the V_2O_3 addition on the structure of the slags, an FT-IR spectral analysis (**Fig. 6**) was carried out on the quenched slag samples. It is worth noting that we

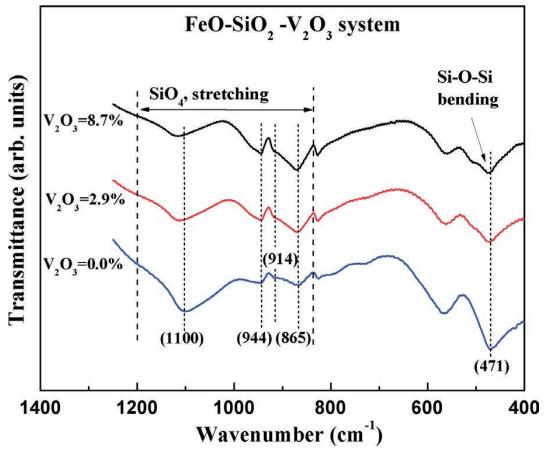

Fig. 6. FT-IR spectra of the quenched samples with different V_2O_3 contents. The FeO/SiO_2 ratio is roughly equal to 1.5 for all samples as indicated in Table 6. (Online version in color.)

only illustrated the spectra of samples containing V_2O_3 up to 8.7%, not 20%, where the MD calculations reached to. This mismatching is because it is difficult to guarantee the slag melt and homogenize completely with the V_2O_3 content increasing at the temperature of 1 550°C. Therefore, only slag samples (glassy state) containing relatively low V_2O_3 content were analyzed here for qualitative investigation.

According to the previous studies,[3,44,45] the vibration region from ~1 200 to ~850 cm^{-1} can be attributed to the symmetric stretching vibration of the SiO_4 tetrahedron. Figure 6 shows that there are four distinct absorption peaks around 1 100, 944, 914 and 865 cm^{-1}, which correspond to Q^3 (NBO/Si=1), Q^2 (NBO/Si=2), Q^1 (NBO/Si=3) and Q^0 (NBO/Si=4), respectively.[46] Relative to the transmittance curve of the V-free slag, the absorption peak for Q^3 (sheet polyanion) at around 1 100 cm^{-1} sequentially damping with increasing the content of V_2O_3, whereas the absorption peak for Q^0 (monomer ployanion) becomes more pronounced. Distinct change of the absorption peaks related to Q^1 and Q^2 could not be obtained from the spectra. In addition, the band near 470 cm^{-1} corresponding to symmetric Si–O bending becomes shallower with increasing the V_2O_3 content, indicating the disappearance of complex silicate structures as suggested by Park *et al.*[47]

Since changes in the intensity of the absorption peaks

at each characteristic wavenumber are associated with the relative variations of the different types of units (Q^n), it can be confirmed that V_2O_3 behaves as a basic oxide which provides O^{2-} to break the inter-tetrahedron connection (Si–O–Si) and then fragment the silicate network.

5. Conclusions

The structural properties of FSV slags with varied content of V_2O_3 at a fixed molar ratio of $FeO/SiO_2=1.5$ were studied using MD simulations and FT-IR analysis. An effective empirical potential was developed for the FSV system as a basis for the MD simulations. Structural information of the short- and medium-range ordering in the FSV slags was obtained. The stable Si–O bond length as well as the 4-fold coordination demonstrates that the SiO_4-tetrahedron is the fundamental ordering units in the slag melts. The local structure surrounding Fe and V shows similar changes with the V_2O_3 addition. Aggregation of ions and performance of coordination between the network-forming Si and Fe were identified. Decrease in averaged Si–O–Si angle as well as the decline of the DOP indicates the structural role of V_2O_3 as a network modifier. FT-IR analysis validated the findings from MD simulations and suggested that V_2O_3 behaves as a basic oxide to fragment the silicate network.

Acknowledgements

This work was financially supported by National Basic Research Program of China (973 Program, grant no. 2013CB632604) and National Natural Science Foundation of China (grant nos. 51090382, 51474041). The authors wish to thank an anonymous reviewer for the critical and helpful comments on the manuscript.

REFERENCES

1) R. R. Moskalyk and A. M. Alfantazi: *Miner. Eng.*, **16** (2003), 793.
2) D. X. Huang: Vanadium Extraction and Steelmaking, Metallurgical Industry Press, Beijing, (2000), 35.
3) I. Sohn and D. J. Min: *Steel Res. Int.*, **83** (2012), 611.
4) K. C. Mills, M. Hayashi, L. Wang and T. Watanabe: Treatise on Process Metallurgy, Vol. 1, ed. by S. Seetharaman, Elsevier, Amsterdam, (2013), 149.
5) H. A. Barolin trans. by C. L. Wang: Oxidation of Vanadium Slag, Metallurgical Industry Press, Beijiing, (1982), 115.
6) I. S. E. Carmichael and M. S. Ghiorso: *Rev. Miner. Geochem.*, **24** (1990), 191.
7) X. Zhang, B. Xie, J. Diao and X. J. Li: *Ironmaking Steelmaking*, **39** (2012), 147.
8) H. X. Fang, H. Y. Li, T. Zhang, B. S. Liu and B. Xie: *ISIJ Int.*, **55** (2015), 200.
9) J. Diao, B. Xie, Y. Wang and C. Q. Ji: *Ironmaking Steelmaking*, **36** (2009), 476.
10) J. Diao, B. Xie, C. Ji, X. Guo and Y. Wang: *Cryst. Res. Technol.*, **44** (2009), 707.
11) P. K. Rao, P. V. R. B. Sarma, A. K. Tripathy and P. K. Jena: *Trans. Inst. Min. Metall. C*, **88** (1979), 187.
12) H. X. Fang: Master thesis, Chongqing University, (2014), 49.
13) Y. Waseda and J. M. Toguri: *Metall. Trans. B*, **9** (1978), 595.
14) S. Rossano, A. Y. Ramos and J. M. Delaye: *J. Non-Cryst. Solids*, **273** (2000), 48.
15) B. O. Mysen and P. Richet: Silicate Glasses and Melts: Properties and Structure, Elsevier, Amsterdam, (2005), 335.
16) W. E. Jackson, F. Farges, M. Yeager, P. A. Mabrouk, S. Rossano, G. A. Waychunas, E. I. Solomon and G. E. Brown: *Geochim. Cosmochim. Acta*, **69** (2005), 4315.
17) H. S. Park, S. S. Park and I. Sohn: *Metall. Mater. Trans. B*, **42** (2011), 692.
18) B. O. Mysen: *Geochim. Cosmochim. Acta*, **70** (2006), 2337.
19) W. G. Seo and F. Tsukihashi: *Mater. Trans.*, **46** (2005), 1240.
20) D. K. Belashchenko and O. I. Ostrovski: *Inorg. Mater.*, **38** (2002), 799.
21) G. Calas and J. Petiau: *Solid State Commun.*, **48** (1983), 625.
22) H. Keppler: *Am. Mineral.*, **77** (1992), 62.
23) G. A. Waychunas, G. E. Brown, C. W. Ponader and W. E. Jackson: *Nature*, **332** (1988), 251.
24) Z. Wang, T. F. Cooney and S. K. Sharma: *Contrib. Miner. Petrol.*, **115** (1993), 112.
25) F. Farges, Y. Lefrère, S. Rossano, A. Berthereau, G. Calas and G. E. Brown: *J. Non-Cryst. Solids*, **34** (2004), 176.
26) G. S. Henderson: *Can. Miner.*, **43** (2005), 1921.
27) K. Zheng, Z. T. Zhang, L. L. Liu and X. D. Wang: *Metall. Mater. Trans. B*, **45** (2014), 1389.
28) S. F. Zhang, X. Zhang, C. G. Bai, L. Y. Wen and X. W. Lv: *ISIJ Int.*, **53** (2013), 1131.
29) H. Hirao and K. Kawamura: Material Design Using Personal Computer, Shokabo, Tokyo, (1994), 52.
30) S. Plimpton: *J. Comput. Phys.*, **117** (1995), 1.
31) P. Norby: *J. Appl. Cryst.*, **30** (1997), 21.
32) H. Fjellvåg, F. Grønvold, S. Stølen and B. Hauback: *J. Solid State Chem.*, **124** (1996), 52.
33) W. Lottermoser, K. Steiner, M. Grodzicki, K. Jiang, G. Scharfetter, J. W. Bats, G. Redhammer, W. Treutmann, S. Hosoya and G. Amthauer: *Phys. Chem. Miner.*, **29** (2002), 112.
34) R. E. Newham and Y. M. De Haan: *Z. Kristallogr. - Cryst. Mater.*, **117** (1962), 235.
35) V. B. Reuter, E. Riedel, V. P. Hug, D. Arndt, U. Geisler and J. Behnke: *Z. Anorg. Allg. Chem.*, **369** (1969), 306.
36) X. H. Huang: Principles of Iron and Steel Metallurgy, Metallurgical Industry Press, Beijing, (2002), 211.
37) J. Du and A. N. Cormack: *J. Non-Cryst. Solids*, **349** (2004), 66.
38) G. S. Henderson, M. E. Fleet and G. M. Bancroft: *J. Non-Cryst. Solids*, **68** (1984), 333.
39) I. Farnan, P. J. Grandinetti, J. H. Baltisberger, J. F. Stebbins, U. Werner, M. A. Eastman and A. Pines: *Nature*, **358** (1992), 31.
40) U. Hoppe, N. P. Wyckoff, M. L. Schmitt, R. K. Brow, A. Schöps and A. C. Hannon: *J. Non-Cryst. Solids*, **358** (2012), 328.
41) G. Ori, M. Montorsi, A. Pedone and C. Siligardi: *J. Non-Cryst. Solids*, **357** (2011), 2571.
42) A. Tilocca, A. N. Cormack and N. H. de Leeuw: *Chem. Mater.*, **19** (2007), 95.
43) Y. Xiang and J. Du: *Chem. Mater.*, **23** (2011), 2703.
44) J. B. Kim and I. Sohn: *ISIJ Int.*, **54** (2014), 2050.
45) S. Ueda, H. Koyo, T. Ikeda, Y. Kariya and M. Maeda: *ISIJ Int.*, **40** (2000), 739.
46) B. O. Mysen, D. Virgo and C. M. Scarfe: *Am. Mineral.*, **65** (1980), 690.
47) J. H. Park, H. Kim and D. J. Min: *Metall. Mater. Trans. B*, **39** (2008), 150.
48) J. Du and L. R. Corrales: *J. Chem. Phys.*, **125** (2006), 114702–1.